Colloid-facilitated release of PFAS from polluted-soil monoliths

Elisabeth Fries, Denis Courtier-Murias, Pierre Labadie, Béatrice Béchet, Pierre-Emmanuel Peyneau, Chloé Caurel, Quentin Dubois, Patrick Pardon, Hélène Budzinski, Eric Michel

Journal of Hazardous Materials 511 (2026) 142279

Contents lists available at ScienceDirect

Journal of Hazardous Materials

journal homepage: www.elsevier.com/locate/jhazmat

Colloid-facilitated release of PFAS from polluted-soil monoliths

Elisabeth Fries [a,b], Denis Courtier-Murias [a], Pierre Labadie [c], Béatrice Béchet [a], Pierre-Emmanuel Peyneau [a], Chloé Caurel [b], Quentin Dubois [c], Patrick Pardon [c], Hélène Budzinski [c], Eric Michel [b,*]

[a] GERS-LEE, Université Gustave Eiffel, Bouguenais F-44344, France
[b] EMMAH, INRAE, Avignon Université, Avignon 84000, France
[c] Université de Bordeaux, UMR CNRS 5805 EPOC, Talence, France

HIGHLIGHTS

- First study investigating colloid-facilitated transport of PFAS in undisturbed soils.
- Colloids increased the mobility of 12 PFAS with 6–11 perfluorinated carbons.
- Diffusion was the rate limiting step for 8 PFAS with 3–7 perfluorinated carbons.
- PFAS content in colloids was up to 25 times higher than in bulk soil.
- Colloidal-phase transfer needs to be considered in models and experimental protocols

GRAPHICAL ABSTRACT

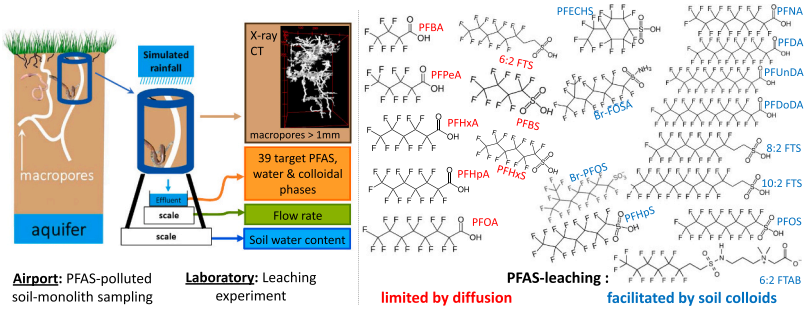

ARTICLE INFO

Keywords:
Forever chemicals
Colloid
Macropore
Undisturbed soil
Transport
Preferential flow
Double-permeability

ABSTRACT

Firefighting Aqueous Film Forming Foams contain per- and polyfluoroalkyl substances (PFAS). Because PFAS are persistent, firefighting training sites constitute a source of soil and groundwater contamination. Colloidal soil particles are known to facilitate the mobility of contaminants that have a strong affinity for soils. Indeed, colloid-facilitated transport of PFAS has been brought up repeatedly to discuss experimental observations regarding PFAS mobility. Still, it has only been observed experimentally for two PFAS molecules, using model experimental situations: repacked soil columns spiked with PFAS. We investigated for the first time the determinants and extent of colloid-facilitated transport of PFAS from AFFF-impacted undisturbed-soil monoliths during simulated rainfalls. These experiments showed that: (i) colloids contributed to the mobility—up to 70% of their concentration in leachates—of 12 PFAS having a perfluorinated carbon chain length $n_c \geq 6$, out of the 20 PFAS present in leachates; (ii) PFAS content in colloids was up to 25 times higher than in bulk soil, this enrichment stemmed from the adsorption on colloids of PFAS present in the soil solution; (iii) colloid-facilitated transport was exacerbated during transient flow regimes, which was probably related to the adsorption of PFAS and colloids to the moving air-water-interfaces. In addition, diffusion was the mechanism limiting the mobility of eight other PFAS with $n_c \leq 7$ and hydrodynamic conditions, linked to the soil structure, strongly affected the mobility of PFAS. The importance of colloidal particles as a carrier phase of PFAS calls for a renewed conceptual model of PFAS fate in soils.

* Corresponding author.
E-mail address: eric.michel@inrae.fr (E. Michel).

https://doi.org/10.1016/j.jhazmat.2026.142279
Received 3 October 2025; Received in revised form 29 April 2026; Accepted 1 May 2026
Available online 4 May 2026

1. Introduction

Per- and polyfluoroalkyl substances (PFAS) refer to a wide family of xenobiotic substances containing at least one perfluorinated methyl (-CF_3) or methylene (-CF_2-) group [1]. PFAS have been used in a wide range of applications since the 1940s [2,3]. They enter the environment through e.g., PFAS production or use sites, waste streams [4,5], municipal sewage sludge applications on agricultural fields [6,7] or the use of aqueous film forming foams (AFFF) designed to extinguish flammable liquid fires [8–10]. In the environment, polyfluoroalkyl substances are eventually metabolized into perfluoroalkyl substances. The latter are persistent in the environment and bioaccumulative [11]. Some PFAS are known to impair the health of living organisms, including humans [11]. The extensive use of these substances together with their persistence result in a widespread occurrence of PFAS in all compartments of the environment [12].

Soils play a key role in the fate of these molecules. They separate the fluxes of water and PFAS between overland flow and infiltration, and they store PFAS, delaying their arrival in aquifers, while allowing them to be internalized by the organisms that live there, such as earthworms and plants [13,14]. Soil contamination by PFAS is thus considered a threat to water resources, soil biota, crops and, ultimately, humans.

For this reason, the mechanisms governing the fate of PFAS in soils have received considerable attention, in particular their sorption and desorption to/from soil constituents (mineral and organic) which control the overall PFAS fluxes from a contamination source, the dissolved plume dynamics, the efficiency of remediation approaches and the bioavailability for plants and soil fauna [15–17]. In situ measurements of PFAS content in the solid phase and in the pore water, as well as laboratory sorption and desorption experiments have led to the determination of soil-water partition coefficients K_d—(mL g^{-1}), the ratio, at equilibrium, of the content of a substance in the soil solid phase (ng g^{-1}) to its concentration in the pore water (ng mL^{-1})—for a number of PFAS [18,19,24]. These coefficients characterize the affinity of PFAS for the soil and are used to evaluate their mobility and parameterize models of PFAS fate. The links between K_d values and molecular properties of PFAS have been studied for several years, showing the importance of solubility and chain length [25,26]. A recent modeling work highlighted that molecular weight and hydrophobicity were the most important PFAS properties for the prediction of their K_d values [27].

Analysis of pore-water and soil PFAS loads at instrumented contaminated sites have also provided insights into mechanisms controlling the mobility of PFAS in soils: (i) mass balance considerations showed that PFAS not only adsorb to soil but also to air water interfaces [19], (ii) the analysis of profiles of PFAS content at a contaminated site showed that PFAS reached greater depths as their molar volumes decreased [20], (iii) simulated irrigation at a contaminated site suggested that out-of-equilibrium processes were at play during PFAS leaching and were more likely linked to a kinetic desorption of PFAS from the soil than to diffusive exchange of water and PFAS between different soil compartments [21].

In addition, since the pioneering work of Murakami et al. [28], PFAS transport experiments have been carried out at the column or lysimeter scale to study the dynamics of PFAS transfers during simulated irrigation events onto columns or lysimeters filled with sand or repacked soils. They confirmed the role of certain factors controlling PFAS sorption in these soils, such as the importance of the perfluoroalkyl chain-length [29] or the soil organic matter content and permitted to explore different ways to model sorption to soil constituents (instantaneous, rate-limited, or a combination of both [22,30,32]. They also revealed other mechanisms affecting the transport of PFAS, such as (i) their adsorption at air-water interfaces [15,22,30,33–37][31], (ii) the possible role of competitive sorption when substances with long perfluoroalkyl chains favor the mobility of substances with shorter chains [36,38], (iii) the possible role of diffusion in controlling short PFAS leaching in soils [39], and (iv) the role of soil colloidal particles in increasing the mobility of PFAS [40–42].

Actually, it has been known since the middle of the 1980s that colloidal soil particles can act as a carrier phase for sorbing pollutants (radionuclides, pesticides, Polycyclic Aromatic Hydrocarbon) that would otherwise be poorly mobile in soils [43]. The possibility of colloid-facilitated transport of PFAS has been explored for the first time during transport experiments in repacked soils spiked with PFOA or PFBA [40,41]. These studies showed that soil colloids did play a significant role in the transport of these molecules, by increasing their leached concentration. The extent of colloid-facilitated transport was found to depend on the PFAS molecule itself, the nature of the colloidal carrier phase and the presence of mobile colloidal particles. More recently, the possibility of colloid-facilitated transport has been hypothesized to explain experimental observations such as unexpectedly high concentration of PFAS in soil leachates [44] or the absence of PFAS in soil profiles [45] Still, to date, the role of colloidal particles on PFAS mobility in soils has not received further attention, in particular to assess the extent of this mechanism and the factors that affect it.

With the exception of a lysimeter study that contained monolithic soil columns [46], all the aforementioned column- and lysimeter-scale experiments focused on model soils, with columns or lysimeters packed with sand or soils previously sieved, that were therefore devoid of structure. However, natural soils exhibit a large distribution of pore sizes, from fine pores within the soil matrix to macropores, caused e.g. by earthworms or decayed roots. This complexity influences the hydrodynamic conditions and *in fine* the transfer processes, e.g. slow diffusive transport through the soil matrix can coexist with fast, gravity-driven preferential macropore flow bypassing most of the soil matrix. This has an impact on contaminant adsorption/desorption and transport, as well as on soil colloid mobilization and transport [47,48]. Furthermore, macropore flow and periods of moderate soil drying are known to favor the mobilization of colloids at the onset of a new rainfall [49–53]. The potential role of macropores has been brought out to explain unexpectedly low PFAS contents in a soil profile [45] or correlations between PFAS and nitrate concentrations [54] as well as discrepancies between PFAS concentrations measured in pore-water collected using a laboratory extraction-protocol and field porous cup suction-lysimeters, suggesting that the latter technique may not be adapted to sample macropore flow [23]. Interestingly, a model of PFAS transport considering macropore flow has been proposed by Zeng and Guo [55], and predicted an acceleration of long chain PFAS release resulting from reduced air-water interfaces in the macropores. To our knowledge, the predictions of this model have not yet been tested against experimental results, probably because the role of macropores in PFAS mobility does not appear to have been the subject of any specific experimental studies.

To address the shortcomings mentioned above, and propose a renewed conceptual model of PFAS fate in structured soils, we explored the combined effects of soil structure, colloid-facilitated transport, and PFAS molecular structure on PFAS release from polluted soils. We performed rainfall simulation experiments on undisturbed soil monoliths excavated at a former firefighting training site contaminated by a cocktail of PFAS due the use of AFFF. To the best of our knowledge, such an experimental situation has never been considered before.

2. Materials and methods

2.1. Sampling of undisturbed soil columns

Four undisturbed soil monoliths (h = 25 cm, inner diameter = 14.5 cm) were sampled in polypropylene cylinders at the former firefighting training site of a major French airport. According to the company managing the airport, the site has been used until 1996 with at least two AFFFs of unknown composition. The columns were sampled by first removing the vegetation (grass) at the soil surface and then gently hammering down the cylinders, that were beveled at their lower end,

into the soil for about 5 cm. The soil around the column was then excavated until reaching the bottom of the cylinder before hammering again the column deeper into the soil. A total of four columns were taken from two positions (hereafter designated as S5 andS8) about 15 m distant along a gradient of soil contamination by PFAS. The two columns taken at each position cannot be considered as replicates but represent examples of the local variability of the macropore network and hydraulic behavior on the sampling site (supplementary material section 7). Two composite bulk soil samples were also collected next to the columns: between 0 and 15 cm and 15 and 25 cm below ground surface. These samples were used to determine the soil characteristics: texture, coarse material content, organic carbon content, pH (Table S5). The soil at both sites is a silt loam (USDA classification). Bulk densities were 1.59 and 1.37 g cm^{-3} at sites S5 and S8 respectively. The fraction of coarse material (> 2 mm) was about 10 times higher in the lower part of both sites than in the first 15 centimeters below surface. At both sampling sites, the pH was 8.1 ± 0.1, consistent with the carbonate concentration. The soil CEC value was comprised in the range of those of kaolinite, 3–15 cmol+ /kg [56]. The mean total organic carbon (TOC) content of the soil was 26 10^{-4} and 37 10^{-4} g g^{-1} for positions S5 and S8 respectively. XRD analysis revealed silicates and calcite minerals (Table S5), reflecting the local geology (limestone rocks, between 2.6% and 10% calcite). Two days after sampling, the internal macropore space of the columns was imaged with an X-ray CT scanner (Siemens Somatom Definition AS) with tube voltage and current of 140 kV and 400 mA respectively. The 3D images (voxel size 300 μm) were processed as described in the supplementary material.

2.2. Rainfall simulation experiments

Rainfall simulation experiments were conducted on the monoliths with a peristaltic pump controlling the rain intensity and duration. One end of a tubing (Ismatec, Tygon 2001, inner diameter 1.02 mm) was connected to the pump, while the second end was supported by a moving 2-axle support located circa 10 cm above the soil surface, permitting to obtain a random pattern of rain droplets (diameter ≈ 2 mm) onto the soil surface. The synthetic rainwater was a 10^{-4} M solution of calcium chloride in ultra-pure water. This concentration was used to reach the ionic-strength of 0.3 mM measured by others in a highly anthropized area, as was the airport site where the monoliths were sampled [57,58]. This value was slightly above the ionic strength of the synthetic rainwater (0.04 mM) used during a PFAS release experiment from repacked soils [22]. A coupling sleeve was used to attach a stainless-steel mesh—with circular 2 mm diameter openings on 42% of its surface area—to the bottom of the columns. During the rainfall experiments, each column was placed onto a stainless-steel funnel. The bottom end of the cores was opened to the atmosphere (free drainage, see supplementary material Section 4). The column weight as well as the weight of the effluent solution at the bottom of the column were recorded every 10 s. These data were used to compute the drainage hydrograph (water flux vs. time) and to determine the temporal evolution of water accumulation within the soil (Fig. S1). It is known that the sampling process increases the soil density close to the walls of the columns, and that wetting and drying cycles lead to a progressive restoration of uniform density in the cores [59,60]. For this reason, four preliminary dry and wet cycles were applied to homogenize the bulk density of each column before the actual rainfall experiment started.

The duration of the rainless period before a rainfall (hereafter referred to as rain interruption duration, RID), is known to affect colloid release when macropore flow occurs [49,51,53]. It has been consistently reported that colloid release increases with the RID until reaching a maximum value for RIDs ranging between 2.5 and 15 days, before decreasing when the RID further increases [49,53,61]. The water flow rate in the soil also affects the release of colloidal particles: high infiltration rates increase colloid release [51,62], and foster macropore flow [48]. Based on the above, to promote colloid release and macropore flow, each soil monolith was subjected to a rainfall experiment occurring 114 h (4.75 days) after the end of the fourth preliminary wetting, at an intensity of 25 mm h^{-1}. The rainfall lasted 48 min, and brought 20 mm of water. Rainfall intensities above 25 mm h^{-1} are in the high range of intensities recorded by the airport weather station within the period of available hourly rainfall data (2005–2022 included) and occurred 13 times. Rainfall events with heights in the range of 20 ± 2 mm during one hour occurred 9 times, essentially between May and September. By comparison, the highest rain height recorded at the weather station during one hour was 27 mm. RIDs of 114 h ± 10% occurred 69 times during the same period. Subsequently, two additional rainfalls, which will not be discussed in this study, were conducted on these columns, after which one column from each site (S5–1 and S8–1) was cut perpendicular to its axis into six slices. The content (ng g^{-1} of soil) of PFAS in these slices, as well as in the effluents (ng mL^{-1} of effluent) from the four columns collected during the three rainfalls, were determined (see next section). These data were used to compute the mass (ng) of each PFAS in the soil at the time it was sliced and the mass (ng) leached during the three rainfalls. This permitted to compute the initial mass (ng) of PFAS prior to the rainfall considered in this study (Fig. S2 and Table S4), as well as the initial PFAS content (ng g^{-1} of soil) at both sites (Table S4).

2.3. Sample preparation and analysis

The column effluents were collected in ten to twelve 25 mL samples, in polypropylene vials throughout the rainfall experiment and drainage. Only two samples may have volumes of effluent lower than 25 mL: the last sample before the rain stopped, because a new vial was used at the beginning of the drainage, and the last sample collected at the end of the drainage. The electrical conductivity and the absorbance at 400 nm of the samples were measured. The absorbance values, measured in 1.5 mL cuvettes, were then transformed into colloidal particle concentrations using an external calibration curve between absorbance values and particle concentrations that was prepared beforehand for the soil of each sampling position [61,63] (see supplementary material section 15). Each collected effluent sample was subdivided into an unprocessed aliquot hereafter named “raw” (1 mL) and a centrifuged aliquot named “supernatant” that was taken after centrifugation of 2 mL the original sample at 20000 × *g* for 20 min (protocol adapted from Borthakur et al. [40,41]). One milliliter of the supernatant was withdrawn. It contained PFAS only in the liquid phase or associated with mineral particles with sizes lower than a calculated cut-off of 37 nm, considering spherical soil mineral particles with a density of 2.6 g cm^{-3} [64]. All water samples were stored at −18 °C until the aliquots were analyzed.

As regards soil samples, a microwave-assisted extraction procedure was used to extract PFAS, followed by graphitized carbon clean-up. Further details are provided in the supplementary material. All samples/extracts were subsequently analyzed using previously established procedures [65,66]. Analysis and quantification of PFAS were performed through liquid chromatography electrospray ionization coupled with tandem mass spectrometry (LC-ESI-MS/MS), using a 1290 liquid chromatography and 6495 triple quadrupole mass spectrometer, both from Agilent Technologies.

The names, acronyms and formula of the targeted compounds are detailed in Table S1, while procedural blanks and limits of detection (LoD) are shown in Table S2 and Table S3 respectively. To maximize the size of the dataset, all samples above the LoD were considered for further analysis. Based on preliminary tests conducted on spiked water and soil samples, a common uncertainty of 15% was assigned to all compounds, for all concentrations, regardless of sample type. It corresponds to the highest relative standard deviation observed in replicate measurements. This conservative choice represents a worst-case scenario.

Subtracting the concentration c_{sup} (ng mL^{-1}) from c_{raw} (ng mL^{-1}), determined by analyzing the supernatant and the raw samples

respectively, permitted to determine the colloid-associated PFAS concentration in the sample; dividing this value by c_{raw} yielded:

$$f_{col} = \frac{c_{raw} - c_{sup}}{c_{raw}} \quad (1)$$

the fraction of PFAS leached that were adsorbed onto colloidal particles. The uncertainties on c_{raw} and c_{sup}, $\sigma_{c_{sup}}$ and $\sigma_{c_{raw}}$ respectively, were propagated to obtain $\sigma_{f_{col}}$, the uncertainty on f_{col} as: $\sigma_{f_{col}} = f_{col}\left(\frac{\sigma^2_{diff}}{diff^2} + \frac{\sigma^2_{c_{raw}}}{c_{raw}{}^2}\right)^{1/2}$, where $diff = c_{raw} - c_{sup}$, and $\sigma^2_{diff} = \sigma^2_{c_{raw}} + \sigma^2_{c_{sup}}$. The PFAS content of the soil colloids (ng mg^{-1} of colloids) can be determined from the colloid concentration in the leachates c_{col} (mg mL^{-1}) as:

$$c_{PFAS,col} = \frac{c_{raw} - c_{sup}}{c_{col}} \quad (2)$$

For each molecule and each sample, we also calculated an apparent partition coefficient $K_{d,soil}$ (mL mg^{-1}) as the ratio of molecule content in soils (c_{soil}, ng mg^{-1} of soil) and leachate concentrations in the supernatant samples (ng mL^{-1}):

$$K_{d,soil} = \frac{c_{soil}}{c_{sup}} \quad (3)$$

An apparent partition coefficient $K_{d,col}$ (mL mg^{-1} of colloids) was also calculated for those samples where colloids contributed to PFAS release ($f_{col} > 0$) as the ratio:

$$K_{d,col} = \frac{c_{PFAS,col}}{c_{sup}} \quad (4)$$

When the remaining volume of the original raw samples (at most 25 mL) was sufficient, measurements of the major elements and TOC were carried out. Eight milliliter samples were analyzed by inductively coupled plasma–optical emission spectroscopy (ICP–OES) according to the standard method ISO 11885:(2007) to determine concentrations of major elements (calcium, potassium, magnesium, sodium, phosphorus, iron and manganese). The raw samples were filtered (0.45 µm syringe filter) and acidified before analysis. The major anions present in the effluents (fluoride, chloride, nitrate, phosphate and sulfate) were quantified by High Performance Ion Chromatrography using a 4-mm AS9HC separation column (Dionex) in suppression mode, at a flow rate if 1 mL min^{-1}. The sample volume was 1.5 mL, of which 25 µL were injected. The raw samples were filtered (0.2 µm syringe filter) before analysis. The total organic carbon of the samples was measured in 10 mL samples with a Vario TOC Cube (Elementar) using the non-purgeable organic carbon method (NF ISO 10694 & NF ISO 13878) [57]. All TOC samples were analyzed twice: before and after being filtered (0.2 µm). When the volume of sample remaining was lower than 10 mL, the samples were diluted with ultrapure water: the sample volume and added water were weighted with a precision scale and the concentration of TOC was back-calculated taking into account the dilution.

3. Results

3.1. Soil contamination

Twenty-five of the thirty-six target molecules were present in contents above detection limits (Table S4). Overall, site S5 was more contaminated than S8. With 706 ng g^{-1}, the sum of PFAS contents at S5 was 26% higher than at S8.

Regardless of the site the two most abundant compounds in the soil were the fluorotelomer 6:2 FTAB (content close to 350 ng g^{-1} of soil) and linear PFOS (L-PFOS, content ranging between 104 and 129 ng g^{-1} of soil). With a content of 21 ng g^{-1} of soil, the third most abundant molecule was PFDA at site S8, and the fluorotelomer 10:2 FTSA at site S5 (65 ng g^{-1} of soil). All perfluoroalkyl carboxylic acids (PFCA) targeted, with a number of perfluorinated carbons n_c ranging between 3 and 13, were quantified. PFDA (n_c = 9) exhibited the highest content at both sites. PFDoA (n_c = 11) and PFUnDA (n_c = 10) were the second most concentrated PFCA at site S5 and S8 respectively. The third most concentrated PFCA was PFPeA (n_c = 4) at S8 and PFUnDA at S5. A short comparison between the contamination measured at this site and that reported at other sites contaminated with AFFF is available in section 5 of the supplementary material.

3.2. Hydrodynamic behavior, effluent conductivity and colloid release

The hydrodynamic behavior of the cores differed considerably depending on the sampling site. For cores from site S8, the drainage flow rate increased rapidly and reached (S8–1) or almost reached—in core S8–2 water accumulated momentarily inside the column—the 25 mm h^{-1} irrigation rate at the soil surface (Fig. 1, Fig. S3, top right panel, black circles). In these cores, the flow rate decreased rapidly after the end of the irrigation. This is in stark contrast with columns from site S5 that showed strong surface water ponding, with maxima outflow rates close to 10 mm h^{-1}, and kept draining during several hours after the irrigation ended (Fig. 1, Fig. S3,top left panel, black circles). These observations are consistent with a qualitative analysis of the 3D images of the soil macropore network of these soil cores. Macropores above the resolution of the images (about three times the voxel size of 300 μm) represented about 2% of the soil volume for cores of position S5, and 4% for cores of position S8. All cores except S5–1 had at least one macropore connecting the soil surface to the bottom end of the cores (Fig. S4 a and b).

The conductivity of the rain water was 26.5 µS cm^{-1}. The conductivity of the effluents was about 500 μS cm^{-1} in the first sample collected for both cores of S5 and 400 µS cm^{-1} for cores of S8 (Fig. 1, Fig. S3, top panel, orange points). The evolution of conductivity differed slightly between each column, but overall, except for S8–2, conductivity was relatively constant and increased during the drainage phase to reach up to 1000 µS cm^{-1} (S5–2). Such values are common for moderately to strongly saline soils [67]. We checked that the conductivity depended on the ions in solution, not on the presence of PFAS counter ions: the molar concentration of the most concentrated PFAS in the leachates (6:2 FTAB, see below) was seven orders of magnitude lower than the lowest molar concentration of nitrate (the predominant anion in the effluents). Accordingly, the evolution of effluent conductivity during the rain experiment was similar to that of the nitrate concentration for all monoliths except S8–2. This was confirmed by linear regressions between conductivity and concentration of nitrate (data not shown): the Pearson correlation coefficient (R^2) was higher than 0.9 (p-value < 0.001) in column S8–1 and S5–2). The linear relationship was weaker for S5–1 ($R^2 > 0.41$, p-values < 0.09). It was not significant for S8–2 that exhibited a constant conductivity.

For all soil cores, the highest colloidal particle concentration was measured in the first effluent sample with values ranging from 2 mg mL^{-1} in core S5–2 to values of 0.8 mg mL^{-1} in core S8–2 (Fig. S3). Particle concentration then decreased rapidly to low values: 0.2 and 0.4 mg mL^{-1} for S5 and S8 cores respectively (Fig. 1, Fig. S3, top panel, blue squares).

The mean TOC concentrations of the unfiltered effluents were 20 and 18 mg L^{-1} for S5–1 and S5–2 respectively, and 23 and 37 mg L^{-1} for S8–1 and S8–2 respectively (Fig S5a). Analysis of TOC in filtered samples revealed that at position S5, 40–43% of the TOC was attributed to colloidal organic carbon (> 0.2 µm) (Fig S5a). The rest was dissolved organic carbon or organic carbon associated to particles < 0.2 µm. Colloidal organic carbon was lower at position S8 (10–27% of the TOC).

3.3. PFAS release

Nineteen of the twenty-five compounds quantified in the soil were found at least in one sample of the column effluents. FOSAA, PFDS, PFTrDA, PFTeDA and FOSA were present in the soil but were not

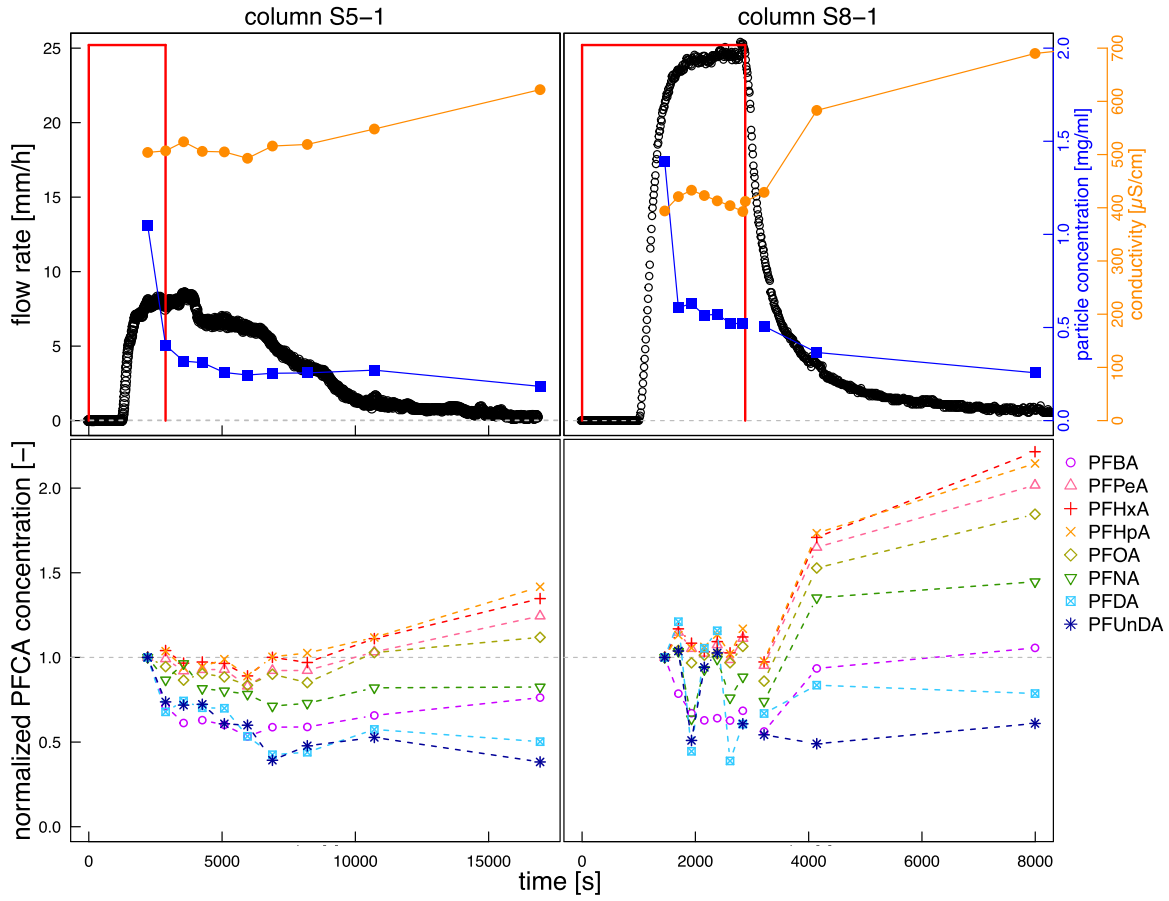

Fig. 1. Rainfall simulation experiments on S5-1 (left panel) and S8-1 (right panel). Upper panel: effluent flow rate (mm h^{-1}, black circles), colloidal particle concentration in the effluents (filled blue squares, mg mL^{-1}) and effluent conductivity (filled orange circles, µS cm^{-1}) as a function of time. The rainfall timing and intensity are indicated as a red rectangle. Bottom panel: normalized PFCA concentrations of the raw samples (c_{raw}) as a function of time. To facilitate the comparison of PFCA concentrations, the concentrations of each molecule was normalized by the concentration of the first effluent sample (non-normalized values are available in Tables S8 and S10). Datapoints were set at the time the samples were collected.

detected in the leachates. PFBS was not detected in the soil but was present in the leachates, probably because the LOD for this substance in solution was very low. Overall, the total mass of PFAS eluted during the rainfall experiments was similar for columns from sites S5 and S8 with an average sum of eluted PFAS masses of 2835 ± 302 ng (Fig. S2). This represents about 0.06% of the PFAS amount (ng) initially present in the soil for monoliths in position S5, and 0.09% in position S8. The most present compounds in the leachates from all columns were 6:2 FTAB followed by PFPeA and L-PFOS.

The release dynamics of the nine PFCA quantified in the effluents ($3 \leq n_c \leq 11$) was different for each compound but appeared to fall into two distinct groups (Fig. 1, Fig. S3, bottom panels). For PFCA with $n_c \leq 7$ (PFBA PFPeA, PFHxA, PFHpA, and PFOA), the concentrations of the samples collected during the falling limb of the hydrograph were up to 2.5 times higher than the concentrations measured during first flow. The latter was not true for PFCA with longer perfluorinated chain lengths ($n_c \geq 9$): their concentration decreased during the experiment compared to first-flow concentration: the higher the carbon number n_c of the molecule, the lower the concentration values reached relative to that at first flow. The release dynamics of PFCA in core S8–2 was markedly different. Its PFCA concentration with $n_c \leq 7$ decreased slightly over the experiment, while that of PFNA and PFDA, $n_c = 8$ and 9 respectively, increased slightly (Fig. S3, lower right panel).

Comparing the upper and lower panels of Fig. 1 and Fig. S3 reveals that for all cores except S8–2, PFCA with perfluorinated chain PFCA with $n_c \leq 7$ appear to follow a release dynamics similar to that of the conductivity. PFCA with $n_c \geq 9$, in contrast, had a release dynamics reminiscent of the colloid release curves (Fig. 1 and Fig. S3). To further quantify these similarities, and extend this analysis to all PFAS found in the effluents, we performed a linear regression between the absolute (non-normalized) concentration of each PFAS and (*i*) the conductivity and (*ii*) the particle concentration measured in the same sample. For all cores, except S8–2, the concentration-conductivity regression was statistically significant (p-value < 0.05) and had a Pearson $R^2 > 0.5$ for PFCA ($4 \leq n_C \leq 7$), PFSA ($4 \leq n_C \leq 6$) and the fluorotelomer 6:2 FTSA (Fig. 2, black dashes and supplementary material, section 14). In column S5–1, the regression between PFAS and colloid concentrations was significant for PFCA ($8 \leq n_C \leq 10$), PFOS ($n_C = 8$) and fluorotelomers (n_C =8 and 10) as well as for perfluorooctane sulfonamide Br-FOSA ($n_C = 8$) (Fig. 2, upper left panel, black + marker). In core S5–2, the regression was significant and had a Pearson $R^2 > 0.5$ for PFUnDA, and the fluorotelomers 6:2 FTAB and 10:2 FTSA (Fig. 2, black + markers). No significant correlations were observed between particle and PFAS concentrations for the cores of site S8 (Fig. 2, right panel).

3.4. Colloid-facilitated PFAS transport

The correlations between colloid and PFAS concentrations suggested the implication of colloidal particle in the release of a number of PFAS molecules. To confirm this hypothesis, we computed for each sample collected the ratio f_{col}, which represents the contribution of colloidal particles to the mobility of PFAS. In the absence of colloid-facilitated transport of PFAS, this ratio was close to zero. We considered only values of f_{col} greater than the uncertainty on f_{col}, which was close to 0.2

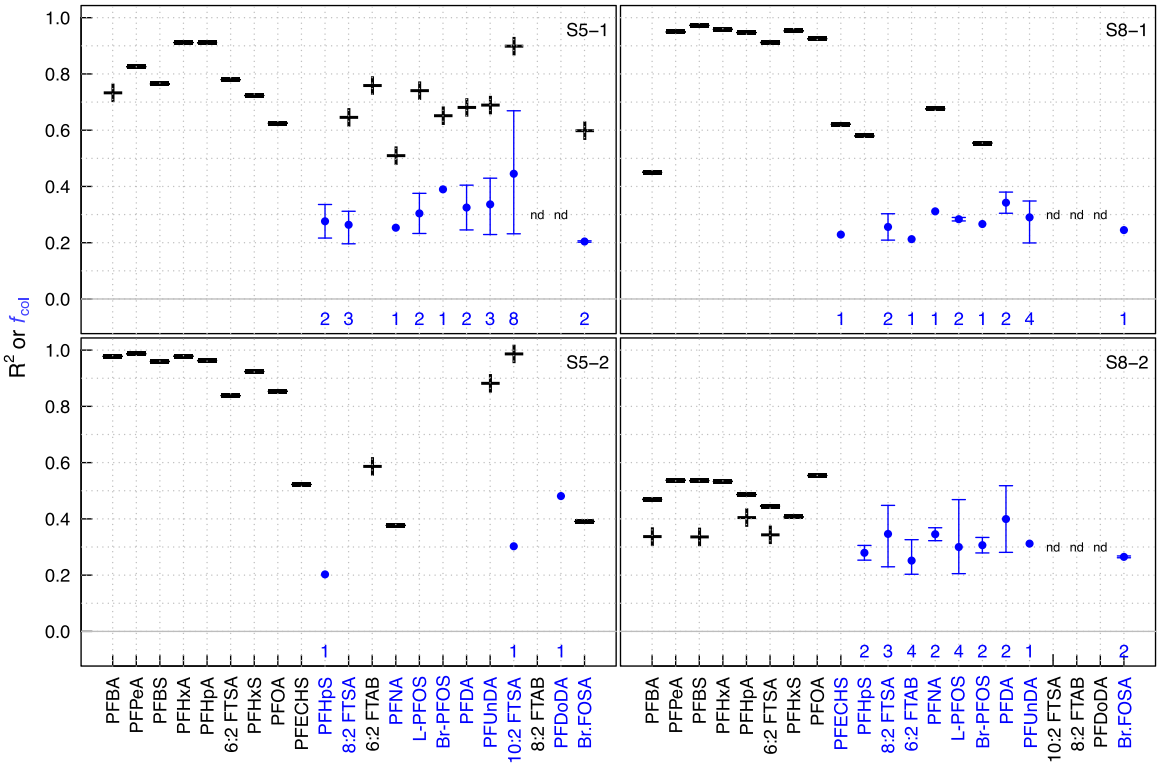

Fig. 2. Pearson correlation coefficients (R^2) obtained from linear regressions between concentrations of each PFCA molecule quantified in the effluent water and (*i*) effluent conductivity (thick black horizontal dashes) or (*ii*) colloidal particle concentration (black +). Only the R^2s for which the regression was significant (p-value < 0.05) are shown. The correlation was not computed when a molecule was detected in less than three effluent samples of a column (nd = not detected is indicated when this occurred). Ratio f_{col} indicating the contribution of the colloidal phase to transfer: mean (blue dots) and maxima and minima values of f_{col} (bars). f_{col} data are available in Table S7. The number of datapoints considered for each substance is indicated in blue type under the horizontal axis. The PFAS are shown in the order of elution from the chromatography column. Substance names written in blue type highlight PFAS that were transported adsorbed onto colloidal particles.

for most samples. Overall, colloids facilitated the transport of 12 PFAS at least in one of the 43 samples collected during the whole experimental campaign (Fig. 2, blue dots representing the mean value of f_{col} and bars representing the extreme values of f_{col} and Table S7). However colloid-facilitated transport was not evenly distributed among the columns or the samples gathered from a given column (Table S7). Colloids facilitated the transfer of nine molecules in cores S5–1, S8–2 and S8–2 but only three in core S5–2 (Table S7). Some of these molecules were consistently detected in samples for individual cores, for example the fluorotelomer 10:2 FTSA that was associated with colloids in eight of the ten effluent samples collected from core S5–1 (Fig. 2, numbers in blue type above the horizontal axis, Table S7).

The substances that were transported on colloids have perfluoroalkyl chain lengths n_c ranging between 6 and 11. They belong to various families: PFCAs (PFNA, PFDA, PFUnDA, PFDoDA), PFSAs (PFHpS, L- and Br-PFOS, PFECHS), derivatives of the perfluorooctane sulfonamide (Br-FOSA), fluorotelomer sulfonates (8:2 FTSA, 10: 2 FTSA), and fluorotelomer sulfonamide alkyl betaines (6:2 FTAB).

For a given molecule, the value of f_{col}, averaged over the entire rainfall, was consistent from one core to the other and ranged between about 0.2 (the lower limit based on the propagated uncertainty on concentration values) and about 0.7 (10:2 FTSA, S5–1, sample 1). f_{col} generally increased with increasing perfluorinated chain lengths n_c (Fig. 2).

For a given monolith, colloid-facilitated transport of PFAS was not evenly distributed during the rainfall. In core S5–1, five and nine different molecules were transported by colloids in the first and penultimate samples, zero to three in the others (Fig. S6a and S6b, upper panel). Similarly, in core S8–2, the transport of four and six molecules was facilitated by colloids in the second and penultimate sample (Fig. S6a and S6b, lower panel). These correspond to the increasing limb of the hydrograph and end of drainage respectively. The same observation applies for S8–2. Overall, the total concentration of colloid-leached PFAS during the rainfall was higher in S8 monoliths, 2.5 and 7.5 ng mL^{-1} for S8–1 and S8–2 respectively, than in S5 monoliths, 1.4 and 0.03 ng mL^{-1} for S5–1 and S5–2 respectively

3.5. Mechanisms of PFAS release

To further explore the mechanisms involved in PFAS release, apparent K_d values were calculated assuming that PFAS molecules in soil and water phases were at equilibrium. The validity of this hypothesis will be discussed later. We computed the apparent partition coefficients $K_{d,soil}$ and $K_{d,col}$ from Eqs. 3 and 4 respectively. Overall, the apparent $K_{d,soil}$ values were about half an order of magnitude above the K_d values measured in ten different soils during batch sorption experiments compiled by Nguyen et al. [18] (Fig. 3).

The $K_{d,soil}$ values were consistent from one column to the other and increased by about half an order of magnitude for each additional CF_2 moieties, for FTSA, PFSA, and to some extent for PFCA, from PFDA to PFUnDA (Fig. 3, error bars). PFCA with $n_c \leq 7$ had $K_{d,soil}$ values about one order of magnitude lower than that of PFDA and did not show any trend with PFCA chain length.

First flow $K_{d,col}$ values (denoted $K_{d,col,first\text{-}flow}$ thereafter) were calculated for the seven compounds for which colloid-facilitated transport was observed during first flow (Fig. 3, filled markers). These $K_{d,col,first\text{-}flow}$ values had the same magnitude and trends as $K_{d,soil}$. This was not true when considering $K_{d,col}$ averaged over all samples where colloid-facilitated transfer occurred: these values lay up to two orders of magnitude above $K_{d,soil}$ values (Fig. 3, open markers).

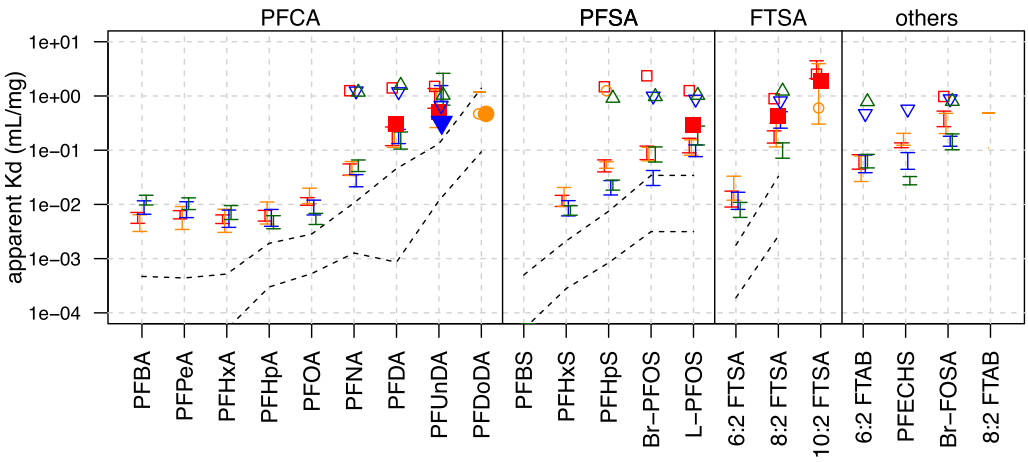

Fig. 3. Apparent soil-water partition coefficient $K_{d,soil}$, and $K_{d,col}$ computed from Eqs. 3 and 4 respectively. Maxima and minima values of $K_{d,soil}$ (bars, colors indicate the column: S5-1: red, S5-2: orange, S8-2: blue and S8-2: green); $K_{d,col}$ values for first flow samples, referred to as $K_{d,col,first\text{-}flow}$ (filled markers); mean $K_{d,col}$ value calculated over all samples for which colloid-facilitated transfer occurred (open markers, S5-1: red squares, S5-2: orange circles, S8-2: blue downward triangles, S8-2: green upward triangle, note that there was no colloid-facilitated transport during first flow for S8-2. The number of values n are indicated for each molecules in Fig. 2. The black dashed lines indicate the minimal and maximal $K_{d,soil}$ values calculated by Nguyen et al. [18], for 10 soils at pH = 7.2, which is similar to the soil pH of this study. Panels from left to right show the K_d values for PFCA, PFSA, FTSA and other substances. The three first panels are ordered by ascending values of the number of perfluorinated carbons.

4. Discussion

In the following, the experimental results gathered in this study will be analyzed and discussed, and, together with salient features of the literature, will be used to propose an improved conceptual model of PFAS fate in undisturbed soils that will be summarized in Fig. 4.

4.1. Soil hydrodynamics and PFAS release

The PFAS contamination in the soil collected at position S5 was 1.5 times higher than that recorded at position S5, with total PFAS masses of 4.8 and 3.2 mg per column respectively (Fig. S2, left panel). However, the eluted PFAS mass during the rainfall experiments was similar for the columns from site S5 and S8 (Fig. S2, right panel). We think that the hydrodynamic behavior of the cores—and hence the structure of the soil pore space—has contributed to this unexpected result. The rapid

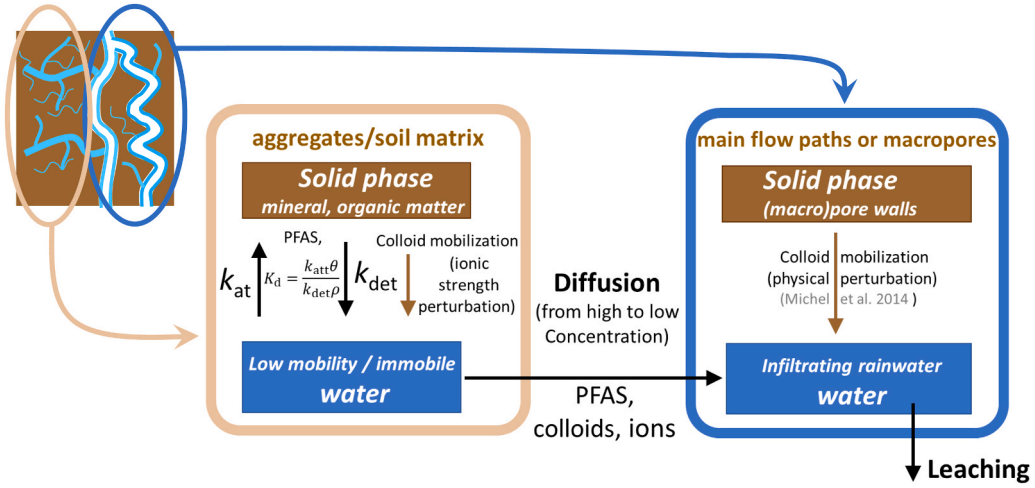

Fig. 4. Conceptual models of (i) soil structure (upper left inset) and of (ii) PFAS mobility in structured soils (bottom right main figure). The soil matrix, often conceptualized as being a packing of soil aggregates, contains most of the surface available for sorption and organic matter (main figure, left panel). The main flow paths conduct the low ionic strength and low PFAS concentration rainwater in the soil porosity (main figure, right panel). In the soil matrix, PFAS are (i) adsorbed onto the soil constituents and (ii) in the soil solution according to their intrinsic K_d values (main figure, left panel). Evidences gathered in this study and others [32, 69] suggest that the equilibrium between PFAS in solution and adsorbed is not reached instantaneously but through a kinetic process conceptualized here by rates of attachment (k_{at}) and detachment (k_{det}) to/from the soil constituents (s^{-1}) that are related to the K_d value through $K_d = (\theta k_{at})/(\rho k_{det})$, where θ is the local water content ($m^3\ m^{-3}$) and ρ the soil bulk density ($kg\ m^{-3}$). For PFAS with a perfluorinated chain length $n_c \leq 8$, the mechanism limiting the leaching is the diffusion from the soil matrix to the water flow path. For compounds with $n_c > 8$, the rate limiting step is no longer diffusion, but either (i) the rate of PFAS desorption to replenish the PFAS concentration in the aggregate pore space that is depleted by diffusion towards the pores conducting infiltrating rainwater or (ii) the diffusion of PFAS-laden colloids. During first flow, colloids are mobilized in the main flow paths by physical perturbations, and in the soil matrix by a decrease in the local ionic strength resulting from the arrival of rainwater. Regardless of their origin, the PFAS load of colloids shortly after mobilization is similar to that of bulk soil. Subsequently, colloids mobilized in the matrix diffuse towards the main flow paths, while acting as sorption sites for PFAS in solution, leading to enrichment of the content of PFAS in colloid compared to bulk soil. The same occurs for first flow colloids mobilized in the main flow pathways, but the enrichment is lower as the residence time of these colloids in the pore water is lower.

variations of outflow rate at the onset and end of the rainfall in cores from position S8 indicate that water transfer was mainly controlled by macropore flow while the strong ponding of water observed on cores from position S5 and the low effluent flow rate suggests that matrix-flow was predominant in these cores (Fig. 1 and Fig. S3). These differences in hydrodynamic behavior led to a globally faster downward movement of water and PFAS in—and out of—S8 cores compared to cores from site S5 [47,48]. This may explain the disproportionally high amount of PFAS leached from S8 compared to S5 monoliths (Fig. S2**,** right panel).

4.2. Leaching dynamics of PFAS with up to 7 perfluorinated carbons

A strong correlation between the leaching dynamics of substances with $n_c \leq 7$ (PFBA, PFPeA and PFHxA, PFHpA, PFOA; PFBS, PFHxS, 6:2 FTSA) and the evolution of effluent conductivity—similar to that of anions such as NO_3^-— was observed (Fig. 2). In a given soil, the conductivity of soil effluents is known to depend on the extent of the soil surface area wetted by the infiltrating water, on the duration of the contact between soil and water, and consequently on the water velocity in the soil pore space [63,68]. The same factors appear to control the leaching of those PFAS molecules that have a moderate affinity for the soil constituents (Fig. 2) and whose content in soil and concentration in pore water reach equilibrium instantaneously or almost instantaneously [39,69]. This suggests that the rate-limiting step for the leaching of PFAS and ions likely originates from the same process. We propose that this process is diffusion, driven by a chemical potential gradient between the small pores in soil aggregates—where most of the surface available for sorption and organic matter are located—and infiltrating rainwater that has a low ionic strength and PFAS concentration [70,71] (Fig. 4). Diffusion-limited leaching is supported by the concomitant increase in effluent conductivity and in concentration of PFAS with $n_c \leq 7$ at the end of drainage, when the largest pores in the soil have already drained, and smaller pores—with lower hydraulic conductivities—are still draining. (Fig. 1 **and** Fig. S3). Diffusion-limited leaching is also supported by the absence of dependence of the apparent $K_{d,soil}$ coefficient for PFCA molecules with $n_c \leq 7$. These findings are consistent with the conceptual model of diffusion-controlled, tracer-like leaching of the shortest PFAS proposed by Schaefer et al. [39].

4.3. Colloid-facilitated transport of PFAS

Substances with $n_c \geq 7$, were present in the AFFF-contaminated soil (Table S4). In spite of their strong affinity for soil constituents, these compounds were detected in the leachates of the columns, except PFTrDA, PFTeDA and PFDS that have a low water solubility and had low content in the soil. The correlation between their release dynamics, especially in cores from position S5, with that of colloidal particle concentration, suggested a role of colloidal particles as a carrier phase of these compounds (Fig. 2). The contribution of colloids was confirmed for twelve molecules by f_{col} values significantly different from zero considering the error on f_{col}. Colloid-facilitated transport was responsible for 20–70% of the concentration of these twelve PFAS in the column effluents (Fig. 2). The remainder probably resulted from their slow desorption in the soil matrix pore space, according to their respective intrinsic K_d values: in the absence of colloid release, the desorption process is the rate-limiting step for these molecules [32] (Fig. 4, main figure, left panel).

In some instances where f_{col} values were different from zero, a correlation with colloid concentration was not observed. This occurred essentially in cores from position S8 where macropore flow was the dominant mechanism of transport. This feature may find a simple explanation when considering that colloid-facilitated transport of a specific molecule often occurred (i) in a small number of samples collected during the rainfall and (ii) at a low value of f_{col} **(**Fig. 2**)**. These few samples and low PFAS load did not have a sufficient weight to induce a linear correlation between the concentrations of a given PFAS and that of colloids. Conversely, in three instances, correlations were observed for specific molecules while no colloid-facilitated transport of PFAS occurred for these molecules (none of the f_{col} values were significantly different from zero). This occurred in cores from position S5 for 6:2 FTAB, PFUnDA and PFBA. This highlights that such correlations are only a hint suggesting the possibility of colloid-facilitated transport, and need to be confirmed by experimental quantification of the actual share of colloidal-phase transport.

4.4. When and why does colloid-facilitated PFAS transport occurs?

The highest colloid concentration was systematically observed in the first effluent sample collected, in line with previous studies on undisturbed soil cores [49,52,53]. In core S5–1, this first flow colloid surge facilitated the release of five molecules (8:2 FTSA, L-PFOS, PFDA, PFUnDA, 10:2FTSA), with a total concentration in the sample of 0.59 ng mL^{-1}, but only one in S5–2 (PFDoDA, 0.01 ng mL^{-1}) and S8–2 (PFUnDA, 0.01 ng mL^{-1}), and none in core S8–2 (Fig. S6a, S6b).

In all cores except S5–1, more substances and higher concentrations of colloid-associated PFAS were leached in the second to fifth samples that corresponded to the increasing limb of the drainage hydrograph and the establishment of a plateau or pseudo-plateau (Fig. S6a, S6b). Such an absence of temporal correlation of colloid and contaminant peaks has been reported by others [72]. We surmise that it results from a difference in colloid size in the first flow sample compared to those collected during the remainder of the rainfall. Indeed, it has been reported that large particles, up to a few tens of micrometers, are leached with the first flow sample, as a consequence of specific mobilization mechanisms acting during first-flow, essentially when macropore flow is dominant [49,50, 62,73]. As large particles have a lower specific surface area than smaller particles, their PFAS load is likely to be lower.

A second surge of colloid-facilitated transport—again not related to a surge in colloid release—was observed in the lower half of the falling limb of the hydrographs (Fig. S6 a, S6 b). Literature suggests that it was probably linked to (i) the scouring of colloids attached to the pore walls during the downward movement of the air water interface (AWI) linked to the drainage front and (ii) the affinity of both PFAS and colloids for AWI [74–77]. We further propose that (iii) the concomitant presence of colloids and PFAS at the AWI may have fostered the sorption of PFAS onto the colloids. Overall, these findings support the analysis of Borthakur et al. [40–42] on the role of the AWI on the mobility of PFAS: the AWI can not only retain PFAS as found by Brusseau et al. [15] but also colloidal particles and their PFAS load, and facilitate the mobility of both, when these interfaces are mobile, during the transient flow regimes of hydrographs.

Colloid-facilitated transport was predominant in monoliths from site S8, dominated by macropore flow, with the two highest sums of colloid-leached PFAS concentrations. This is consistent with the characteristics of the macropore network (Table S6) and a large body of literature on colloid transport in undisturbed soils showing that macropore flow facilitates the release of colloids [49,53]. Still, with a sum of concentrations 1.4 ng mL^{-1}, core S5–1 showed significant colloid-facilitated transport. This is surprising because this core has no percolating macropore above the X-ray CT image resolution, and exhibited the strongest ponding of the cores from site S5. We surmise that the slow water flow and water accumulation in —and at the surface of— soil core S5–1 may have allowed sufficient time for the mobilization and diffusion of colloids with adsorbed PFAS from the aggregate porosity into the water outflow pathways (Fig. 4).

4.5. Insights on PFAS retention and release mechanisms inferred from apparent K_d values

The increase of the apparent $K_{d,soil}$ values by about half an order of magnitude for each additional CF_2 moieties observed for PFCA with $n_c \geq 8$, and for PFSA and FTSA with $n_c \geq 6$ (Fig. 3**)** indicates that the

perfluoroalkyl chains were involved in sorption for these PFAS, likely through hydrophobic interactions.

Calculated K_d values were about half an order of magnitude above those reported by Nguyen et al. [15], during batch sorption experiments, on a substance-by-substance basis, for ten soils of different characteristics. This indicates that the concentration c_{sup} of PFAS in solution (ng mL^{-1}, see Eqs. 3 and 4) was lower than expected from these literature-based K_d values and the soil content c_{soil} (ng g^{-1}). One possible explanation may be that the experimental conditions were vastly different in our study compared to those of Nguyen et al. [18]: aged contamination vs. freshly spiked soil, desorption vs. sorption, presence of a cocktail of molecules vs. a single molecule, soil monolith vs. batch. In particular, we propose that the soil structure may have the greatest contribution to such low c_{sup} values. In a common conceptual model of soil structure, water can be found in different compartments: (*i*) inside the soil aggregates or the soil matrix, where water has a low mobility, and (*ii*) in the main pores or macropores were water infiltrates [78]. Both compartments are connected by diffusive water and solute transfer (Fig. 4). In our experiments, we measured the concentration of PFAS c_{sup} in the column effluents, mainly connected to the latter compartment. Although equilibrium between aqueous and solid phase may have been reached in the former compartment, the high K_d values, compared to those of Nguyen et al. [18], suggest that the 114 h-long dry period preceding the onset of the rainfall was not long enough to let (i) substances with $n_c \leq 7$ diffuse sufficiently towards the paths followed by infiltrating rainwater and (ii) longer chain PFAS desorb sufficiently from the soil constituents and diffuse towards the same flow paths, to reach equilibrium between the outflow water and the soil content, leading to K_d values higher than those expected from the literature.

Interestingly, (i) the apparent $K_{d,soil}$ values coincided within a factor of three with $K_{d,col,first\text{-}flow}$ computed from colloid release during first flow while (ii) $K_{d,col,}$—computed from all samples when colloids were involved in PFAS release was observed—were higher, up to two orders of magnitude, than $K_{d,col,first\text{-}flow}$ (Fig. 3 open markers). A comparison of Eqs. 3 and 4 indicates that the similarity of $K_{d,soil}$ and $K_{d,col,first\text{-}flow}$ values (and the dissimilarity between $K_{d,col,first\text{-}flow}$ and $K_{d,col}$) must stem from the similarity (or dissimilarity) of PFAS contents in the immobile soil and mobile colloids, c_{soil} and $c_{PFAS,col}$ respectively.

4.6. PFAS are enriched in colloids compared to bulk soil

To further characterize the colloid PFAS load, we computed the content of each PFAS adsorbed on colloidal particles ($c_{PFAS,col}$, ng g^{-1} of colloid, Eq. 2) and compared it to its content in the immobile soil (c_{soil}) through the ratio $c_{PFAS,col}/c_{soil}$. A ratio higher than one indicates an enrichment of PFAS in the colloids compared to the bulk immobile soil. These enrichment data (Fig. S7) revealed that (i) as expected from the $K_{d,col}$ values (Fig. 3), the PFAS content was higher —up to 25 times— in the colloidal phase than in the immobile bulk soil, and (ii) in colloids, short molecules were more concentrated than longer ones: the available data suggest that the enrichment factor decreased exponentially with the perfluorinated chain length (Fig. S7).

Several mechanisms acting separately or jointly may help understanding these results. As proposed by Borthakur et al. [40]), the high specific surface area of colloidal particles allows the sorption of PFAS to higher contents than in the bulk soil. Additionally, the nature of colloidal particles and in particular their organic carbon content may further enhance the sorption of PFAS. To test this hypothesis, we compared the TOC content of the colloids to that of bulk soil and found that colloids leached from cores of site S5 did have a TOC content up to 3 times higher than the bulk soil, while those leached from site S8 cores had a TOC about half that of the bulk soil (Fig. S5 **b**). Still, PFAS enrichment was observed regardless of the origin of the monoliths, so the TOC content of the colloids is probably not a key factor controlling PFAS enrichment in colloids.

We propose that the mobilization of colloidal particles at different locations within the soil, through different mobilization mechanisms, may help understanding the set of observations mentioned above. Several studies have suggested that colloidal particles leached during first flow are mobilized by physical mechanisms (inertial forces, capillary forces, differential stresses) in the macropores and main pores conducting water (Fig. 4, main figure, right panel), [50,61,62,74,79]. The residence time of these freshly mobilized colloids in the macropores and main flow paths is short. It allows only moderate kinetic adsorption [32,69] onto the colloids, of the PFAS present in the soil solution. Consequently, first-flow colloids have a PFAS-load close to that of bulk soil as observed in Fig. 3 (filled markers). By contrast, the mobilization of colloidal particles farther from these pores, in the soil matrix or inside the soil aggregates (Fig. 4, main figure, left panel), is most likely linked to a decrease in ionic strength of the local soil solution, altering the balance between the attractive and repulsive forces (van der Waals and electrostatic respectively) controlling the mobility of colloidal particles [80]. Once mobilized, these colloids diffuse towards the main flow paths, a slow process allowing time for the kinetic sorption [32,69] of PFAS present in the soil solution in concentrations determined by their intrinsic K_d values and the soil content. As previously mentioned, these K_d values are mainly influenced by hydrophobicity and molecular weight concerning PFAS properties. Soil characteristics also play an important role with organic carbon content being the predominant factor influencing sorption of PFAS [27].

Interestingly, within each PFAS subgroup, PFAS enrichment on colloids decreased exponentially with increasing perfluoroalkyl chain length n_c, (Fig. S7, right panel): the opposite was expected as the affinity of PFAS for soil constituents (and thus also for colloids) increases with each additional $–CF_2–$ moieties by about half an order of magnitude. Still, the extent of sorption depends not only on the affinity of a chemical for the sorbent, but also on its availability in solution. The availability of PFAS in solution decreases as n_c increases [18]. This may explain the decreasing exponential relationship between colloid enrichment and n_c: it mirrors the increasing exponential relationship between n_c and K_d values observed for PFAS with $n_c > 7$ in this study (Fig. 3) and elsewhere [18].

4.7. Limits and implications of this study

The possibility of PFAS transport in colloidal phase raises issues regarding PFAS analysis protocols and the interpretation of previous experimental work. In some early studies on PFAS contamination of groundwater or soil leachates, water samples were filtered or centrifuged before PFAS extraction, precluding the possibility to monitor colloid-borne substances such as long-chain PFAS [6,81]. Their absence was explained by their high affinity for soil constituents [82] or the formation of non-extractable residues [38], but our results point out that they may have been removed by the sample preparation process. It is therefore necessary to consider past results and interpretations with care and to develop water analysis protocols that include the extraction of colloid-bound PFAS.

In the same vein, we would like note that an important body of literature reports field sampling of pore water using suction lysimeters [19,21,23,24,83,84]. However, in addition to their intrinsic limitations to sample water from macropores, “unless the macropores are directly intercepted” by the porous cup [85], the porous ceramics may act as a filter (pore size of 1.4 μm for a bubbling pressure of 2 bars) preventing the sampling of colloidal particles —and sorbed PFAS—above the ceramic pore size.

In this study, and in the pioneering work by Borthakur et al. [40], colloid-bound PFAS were separated from PFAS in solution by centrifugation. We believe that this method should be preferred over filtration, as (i) it has been shown that PFAS bind to most filters [86] and (ii) centrifugation eliminates the need to adhere to the size cutoffs set by the availability of filters making it possible to quantify truly dissolved PFAS

(see supplementary material section 16). Centrifugation is based on a density difference between colloidal particles and water. Considering mineral colloids with a density of 2.6 g cm^{-3} lead to a calculated cut-off of about 37 nm. Still, colloidal organic-matter has a lower density and consequently a higher particle size cut-off. For this reason, in this study, as well as in Borthakur et al. [40], if colloidal organic matter alone (i.e., not adsorbed onto mineral particles) did contribute to PFAS release, its contribution was accounted for in solution phase. This may explain why in some leachate samples the concentration of PFAS such as Br-FOSA was higher in the supernatant of the centrifuged sample than in the raw, uncentrifuged one (Table. S8). As a consequence, the extent of colloid-facilitated transport of PFAS presented here likely constitutes a lower bound for the real contribution of colloids to the mobility of PFAS. Finally, the small quantity of colloidal particles collected in the samples did not permit a physical and chemical characterization and fractionation of the colloidal phase. Such characterization should be carried-out in future studies.

5. Conclusion

This study investigated the role of soil colloids and macropores in the release of PFAS from contaminated and undisturbed soil monoliths excavated at a former firefighter training site. This experimental situation, lying half-way between experiments in packed soil columns and field studies, permitted to quantify for the first time the integral role played by soil colloids in the mobility of PFAS through undisturbed soils:

- Colloids facilitated the release of 12 PFAS having perfluorinated chain lengths ranging between 6 and 11 carbon atoms. Eight of these substances were perfluoroalkyl acids, one was a derivative of perfluorooctanesulfonamide, and three were fluorotelomers.
- Colloids contributed up to 70% of the concentration of these substances in leachates. The remainder resulted from the kinetic desorption of these substances according to their respective affinity for soil constituents.
- Colloid-facilitated transfer was observed during most of each rainfall but was more important during the transient phases of the hydrographs that coincided with the passage of the air-water interfaces associated with the infiltration and drainage fronts.
- PFAS content in colloids was higher than in bulk soil. The enrichment of the colloidal phase depended on the perfluorinated chain length n_c of the PFAS (it decreased exponentially with n_c) and was likely due to the adsorption of PFAS molecules present in the soil solution onto colloids.

The experiments also suggested that diffusion—and not desorption—was the mechanism controlling the mobility of eight other substances with up to 7 perfluorinated carbon atoms.

These findings led to a renewed conceptual model of PFAS fate in soils: their mobility depends not only on their affinity for soil components and air-water interfaces, but also on the mechanisms controlling the mobilization, stability and transport of colloids. They also pointed out the need to adapt analytical measurement protocols for PFAS in water samples: they should include the extraction of PFAS from colloidal particles to avoid underestimating the total PFAS concentration.

Overall, this study provided an improved understanding of the dominant PFAS fate mechanisms in undisturbed soils. This constitutes a key step towards the implementation —and parameterization— of more generic models to predict the persistence of PFAS at a contaminated source area as well as their release towards groundwater and their bioavailability for the soil fauna and crops.

Environmental Implication

This study showed that colloidal soil particles facilitated the transport of long-chain per- and polyfluoroalkyl substances (PFAS) which—because of their affinity for the soil mineral and organic constituents—would otherwise be poorly mobile. As observed for other contaminants, this transport mechanism was predominant at the beginning and end of a rainfall and when the hydrodynamics of the soil was dominated by macropore flow. These findings helped explaining the presence of long-chain PFAS in groundwater, led to a renewed conceptual model of PFAS fate in undisturbed soils and called for analysis protocols that include the extraction of colloid-bound PFAS.

CRediT authorship contribution statement

Hélène Budzinski: Writing – review & editing, Resources. **Quentin Dubois:** Writing – review & editing, Investigation, Formal analysis. **Patrick Pardon:** Validation, Investigation. **Pierre-Emmanuel Peyneau:** Writing – review & editing, Validation, Formal analysis. **Chloé Caurel:** Writing – review & editing, Visualization, Software, Formal analysis. **Pierre Labadie:** Writing – review & editing, Validation, Supervision, Resources, Methodology. **Béchet Béatrice:** Writing – review & editing, Validation, Methodology. **Elisabeth Fries:** Writing – review & editing, Writing – original draft, Visualization, Software, Investigation, Formal analysis. **Denis Courtier-Murias:** Writing – review & editing, Supervision, Methodology, Formal analysis, Conceptualization. **Eric Michel:** Writing – review & editing, Writing – original draft, Visualization, Validation, Supervision, Software, Resources, Project administration, Methodology, Funding acquisition, Formal analysis, Data curation, Conceptualization.

Declaration of Competing Interest

The authors declare the following financial interests/personal relationships which may be considered as potential competing interests: Eric Michel reports financial support was provided by The French Agency for Ecological Transition. If there are other authors, they declare that they have no known competing financial interests or personal relationships that could have appeared to influence the work reported in this paper.

Acknowledgments

The authors would like to thank ADEME, the French Agency for Ecological Transition for financial support through the IPANEMA project, contract 2172D0213. E. Fries was supported by a joint PhD grant funded by the Agroecosystem division of INRAE and by Université Gustave Eiffel. We also thank: the company that manages the airport for granting us the permission to extract soil cores at their former firefighting training site, and in particular D. Cohen-Solal for his help during sampling, as well as H. Carronnier from Valgo for setting up this collaboration; Météo France for providing the meteorological records at the airport site; H. Adriensen, F. Lecompte and F. Elleboudt from the imaging platform PIXANIM for performing the acquisition of the X-ray CT 3D images of the soil cores; F. Tison from INRAE EMMAH for designing and assembling the two axel moving rainfall simulator as well as the automated leachate-sample collector, L. Capowiez from INRAE EMMAH, who helped setting up the ion chromatography analyses; M. Palhec, S. Negro and J. Fouche from INRAE LISAH for performing the TOC measurements. M. Guillon and N. Caubrière from GERS-EE are also acknowledged for ICP-OES. PFAS analyses were performed thanks to The PLATINE platform (Organic Environmental Analytical Chemistry Platform) at UMR 5805 EPOC that provided the analytical facilities. Finally, the authors would like to thank the two reviewers whose questions and comments helped improve the manuscript.

Appendix A. Supporting information

Supplementary data associated with this article can be found in the online version at doi:10.1016/j.jhazmat.2026.142279.

Data Availability

Data will be made available on request.

References

[1] OECD, 2021. Reconciling terminology of the universe of per-and polyfluoroalkyl substances: Recommendations and practical guidance. OECD Series on Risk Management of Chemicals. OECD Publishing, Paris. https://doi.org/10.1787/e458e796-en.

[2] Prevedouros, K., Cousins, I.T., Buck, R.C., Korzeniowski, S.H., 2006. Sources, fate and transport of perfluorocarboxylates. Environ Sci Technol 40 (1), 32–44 doi: 10.1021/es0512475.

[3] Buck, R.C., Franklin, J., Berger, U., Conder, J.M., Cousins, I.T., Voogt, P.D., et al., 2011. Perfluoroalkyl and polyfluoroalkyl substances in the environment: Terminology, classification, and origins. Integr Environ Assess Manag 7 (4), 513–541. https://doi.org/10.1002/ieam.258.

[4] Bach, C., Dauchy, X., Boiteux, V., Colin, A., Hemard, J., Sagres, V., et al., 2017. The impact of two fluoropolymer manufacturing facilities on downstream contamination of a river and drinking water resources with per- and polyfluoroalkyl substances. Environ Sci Pollut Res 24 (5), 4916–4925. https://doi.org/10.1007/s11356-016-8243-3.

[5] Liu, S., et al., 2023. Transport and transformation of perfluoroalkyl acids, isomer profiles, novel alternatives and unknown precursors from factories to dinner plates in China: New insights into crop bioaccumulation prediction and risk assessment (January). Environ Int 172, 107795. https://doi.org/10.1016/j.envint.2023.107795.

[6] Washington, J.W., Yoo, H., Ellington, J.J., Jenkins, T.M., Libelo, E.L., 2010. Concentrations, distribution, and persistence of perfluoroalkylates in sludge-applied soils near Decatur, Alabama, USA. Environ Sci & Technol 44 (22), 8390–8396. https://doi.org/10.1021/es1003846.

[7] Munoz, G., Michaud, A.M., Liu, M., Vo Duy, S., Montenach, D., Resseguier, C., et al., 2022. Target and nontarget screening of PFAS in biosolids, composts, and other organic waste products for land application in France. Environ Sci Technol 56 (10), 6056–6068. https://doi.org/10.1021/acs.est.1c03697.

[8] Guelfo, J.L., Higgins, C.P., 2013. Subsurface transport potential of perfluoroalkyl acids at aqueous film-forming foam (AFFF)-impacted sites. Environ Sci Technol 47 (9), 4164–4171. https://doi.org/10.1021/es3048043.

[9] Barzen-Hanson, K.A., Roberts, S.C., Choyke, S., Oetjen, K., Mcalees, A., Riddell, N., et al., 2017. Discovery of 40 classes of per- and polyfluoroalkyl substances in historical aqueous film-forming foams (AFFFs) and AFFF-impacted groundwater. Environ Sci Technol 51 (4), 2047–2057. https://doi.org/10.1021/acs.est.6b05843.

[10] Liu, M., Munoz, G., Vo Duy, S., Sauvé, S., Liu, J., 2021. Per-and polyfluoroalkyl substances in contaminated soil and groundwater at airports: a Canadian case study. Environ Sci Technol 56 (2), 885–895. https://doi.org/10.1021/acs.est.1c04798.

[11] Lyu, X., Xiao, F., Shen, C., Chen, J., Park, C.M., Sun, Y., et al., 2022. Per-and polyfluoroalkyl substances (PFAS) in subsurface environments: occurrence, fate, transport, and research prospect. Rev Geophys 60 (3) e2021RG000765.

[12] Cousins, I.T., Johansson, J.H., Salter, M.E., Sha, B., Scheringer, M., 2022. Outside the safe operating space of a new planetary boundary for per- and polyfluoroalkyl substances (PFAS). Environ Sci Technol 56 (16), 11172–11179. https://doi.org/10.1021/acs.est.2c02765.

[13] Delor, L., Louzon, M., Pelosi, C., Michel, E., Maillet, G., Carronnier, H., 2023. Ecotoxicity of single and mixture of perfluoroalkyl substances (PFOS and PFOA) in soils to the earthworm Aporrectodea caliginosa. Environ Pollut, 122221. https://doi.org/10.1016/j.envpol.2023.122221.

[14] Ghisi, R., Vamerali, T., Manzetti, S., 2019. Accumulation of perfluorinated alkyl substances (PFAS) in agricultural plants: a review. Environ Res 169, 326–341. https://doi.org/10.1016/j.envres.2018.10.023.

[15] Brusseau, M.L., 2018. Assessing the potential contributions of additional retention processes to PFAS retardation in the subsurface. Sci Total Environ 613-614, 176–185. https://doi.org/10.1016/j.scitotenv.2017.09.065.

[16] Travar, I., Uwayezu, J.N., Kumpiene, J., Yeung, L.W., 2020. Challenges in the PFAS remediation of soil and landfill leachate: a review, 1–1 Adv Environ Eng Res 02 (02). https://doi.org/10.21926/aeer.2102006.

[17] Bolan, N., et al., 2021. Remediation of poly- and perfluoroalkyl substances (PFAS) contaminated soils – To mobilize or to immobilize or to degrade? J Hazard Mater 401, 123892. https://doi.org/10.1016/j.jhazmat.2020.123892.

[18] Nguyen, T.M.H., Bräunig, J., Thompson, K., Thompson, J., Kabiri, S., Navarro, D. A., et al., 2020. Influences of chemical properties, soil properties, and solution ph on soil–water partitioning coefficients of per- and polyfluoroalkyl substances (PFASs). Environ Sci Technol 54 (24), 15883–15892. https://doi.org/10.1021/acs.est.0c05705.

[19] Schaefer, C.E., Lavorgna, G.M., Lippincott, D.R., Nguyen, D., Christie, E., Shea, S., et al., 2022. A field study to assess the role of air-water interfacial sorption on PFAS leaching in an AFFF source area. J Contam Hydrol 248, 104001.

[20] Bigler, M.C., Brusseau, M.L., Guo, B., Jones, S.L., Pritchard, J.C., Higgins, C.P., et al., 2024. High-resolution depth-discrete analysis of PFAS distribution and leaching for a vadose-zone source at an AFFF-Impacted site. Environ Sci Technol 58 (22), 9863–9874.

[21] Schaefer, C.E., Lavorgna, G.M., Lippincott, D.R., Nguyen, D., Schaum, A., Higgins, C.P., et al., 2023. Leaching of perfluoroalkyl acids during unsaturated zone flushing at a field site impacted with aqueous film forming foam. Environ Sci Technol 57 (5), 1940–1948.

[22] Shea, S.M., Schaefer, C.E., Illangasekare, T., Higgins, C.P., 2025. Release of poly- and perfluoroalkyl substances from AFFF-impacted soils: effects of water saturation in vadose zone soils. J Contam Hydrol 269, 104506.

[23] Schaefer, C.E., Nguyen, D., Fang, Y., Gonda, N., Zhang, C., Shea, S., et al., 2024. PFAS Porewater concentrations in unsaturated soil: field and laboratory comparisons inform on PFAS accumulation at air-water interfaces. J Contam Hydrol 264, 104359.

[24] Pritchard, J.C., Hire, M., McDonough, J., Higgins, C.P., Schaefer, C.E., 2025. PFAS conceptual site model of an AFFF-impacted firefighting training area informed by high resolution soil, porewater, and groundwater sampling. J Contam Hydrol, 104728.

[25] Liu, J., Lee, L.S., 2005. Solubility and sorption by soils of 8: 2 fluorotelomer alcohol in water and cosolvent systems. Environ Sci Technol 39 (19), 7535–7540.

[26] Liu, J., Lee, L.S., 2007. Effect of fluorotelomer alcohol chain length on aqueous solubility and sorption by soils. Environ Sci Technol 41 (15), 5357–5362.

[27] Fabregat-Palau, J., Ershadi, A., Finkel, M., Rigol, A., Vidal, M., Grathwohl, P., 2025. Modeling PFAS sorption in soils using machine learning. Environ Sci Technol 59 (15), 7678–7687. https://doi.org/10.1021/acs.est.4c13284.

[28] Murakami, M., Sato, N., Anegawa, A., Nakada, N., Harada, A., Komatsu, T., et al., 2008. Multiple evaluations of the removal of pollutants in road runoff by soil infiltration. Water Res 42 (10-11), 2745–2755.

[29] Stahl, T., Riebe, R.A., Falk, S., Failing, K., Brunn, H., 2013. Long-term lysimeter experiment to investigate the leaching of perfluoroalkyl substances (PFASs) and the carry-over from soil to plants: results of a pilot study. J Agric Food Chem 61 (8), 1784–1793.

[30] Lyu, Y., Brusseau, M.L., Chen, W., Yan, N., Fu, X., Lin, X., 2018. Adsorption of PFOA at the air–water interface during transport in unsaturated porous media. Environ Sci Technol 52 (14), 7745–7753. https://doi.org/10.1021/acs.est.8b02348.

[31] Brusseau, M.L., Van Glubt, S., 2019. The influence of surfactant and solution composition on PFAS adsorption at fluid-fluid interfaces. Water Res 161, 17–26. https://doi.org/10.1016/j.watres.2019.05.095.

[32] Maizel, A.C., Shea, S., Nickerson, A., Schaefer, C., Higgins, C.P., 2021. Release of per- and polyfluoroalkyl substances from aqueous film-forming foam impacted soils. Environ Sci Technol 55 (21), 14617–14627. https://doi.org/10.1021/acs.est.1c02871.

[33] Costanza, J., Arshadi, M., Abriola, L.M., Pennell, K.D., 2019. Accumulation of PFOA and PFOS at the Air-Water Interface. Environ Sci Technol Lett 6 (8), 487–491. https://doi.org/10.1021/acs.estlett.9b00355.

[34] Brusseau, M.L., Van Glubt, S., 2021. The influence of molecular structure on PFAS adsorption at air-water iMcnterfaces in electrolyte solutions. Chemosphere 281 (May), 130829. https://doi.org/10.1016/j.chemosphere.2021.130829.

[35] Brusseau, M.L., Guo, B., 2022. PFAS concentrations in soil versus soil porewater: Mass distributions and the impact of adsorption at air-water interfaces. Chemosphere, 138954. https://doi.org/10.1016/j.chemosphere.2022.134938.

[36] Gellrich, V., Stahl, T., Knepper, T., 2012. Behavior of perfluorinated compounds in soils during leaching experiments. Chemosphere 87 (9), 1052–1056. https://doi.org/10.1016/j.chemosphere.2012.02.011.

[37] Hubert, M., Bonnet, B., Hale, S.E., Sørmo, E., Cornelissen, G., Ahrens, L., et al., 2025. Measurement and modelling of sorbent-amendment impacts on seasonal and long-term PFAS transport through unsaturated soil lysimeters. J Hazard Mater, 138662.

[38] McLachlan, M.S., Felizeter, S., Klein, M., Kotthoff, M., De Voogt, P., 2019. Fate of a perfluoroalkyl acid mixture in an agricultural soil studied in lysimeters. Chemosphere 223, 180–187. https://doi.org/10.1016/j.chemosphere.2019.02.012.

[39] Schaefer, C.E., Nguyen, D., Christie, E., Shea, S., Higgins, C.P., Field, J.A., 2021. Desorption of poly- and perfluoroalkyl substances from soil historically impacted with aqueous film-forming foam. J Environ Eng 147 (2), 06020006. https://doi.org/10.1061/(ASCE)EE.1943-7870.0001846.

[40] Borthakur, A., Cranmer, B.K., Dooley, G.P., Blotevogel, J., Mahendra, S., Mohanty, S.K., 2021. Release of soil colloids during flow interruption increases the pore-water PFAS concentration in saturated soil. Environ Pollut 286, 117297. https://doi.org/10.1016/j.envpol.2021.117297.

[41] Borthakur, A., Olsen, P., Dooley, G.P., Cranmer, B.K., Rao, U., Hoek, E.M., et al., 2021. Dry-wet and freeze-thaw cycles enhance PFOA leaching from subsurface soils. J Hazard Mater Lett 2, 100029. https://doi.org/10.1016/j.hazl.2021.100029.

[42] Borthakur, A., Wang, M., He, M., Ascencio, K., Blotevogel, J., Adamson, D.T., et al., 2021. Perfluoroalkyl acids on suspended particles: significant transport pathways in surface runoff, surface waters, and subsurface soils. J Hazard Mater 417, 126159. https://doi.org/10.1016/j.jhazmat.2021.126159.

[43] McCarthy, J., Zachara, J.M., 1989. Subsurface transport of contaminants: mobile colloids in the subsurface environment may alter the transport of contaminants. Environ Sci Technol 23, 5. https://doi.org/10.1021/es00065a001.

[44] Bierbaum, T., Hansen, S.K., Poudel, B., Haslauer, C., 2023. Investigating rate-limited sorption, sorption to air–water interfaces, and colloid-facilitated transport during PFAS leaching. Environ Sci Pollut Res 30 (58), 121529–121547. https://doi.org/10.1007/s11356-023-30811-2.

[45] Peter, L.G., Lee, L.S., Burbage, C., Hoffman, K., Richardson, A., 2025. PFAS retention and distribution in the vadose zone of three soil types impacted by biosolids application. J Environ Manag 396, 128137.

[46] Stahl, T., Riebe, R.A., Falk, S., Failing, K., Brunn, H., 2013. Long-term lysimeter experiment to investigate the leaching of perfluoroalkyl substances (PFASs) and

the carry-over from soil to plants: results of a pilot study. J Agric Food Chem 61 (8), 1784–1793.
[47] Jarvis, N., 1998. Modelling the impact of preferential flow on nonpoint source pollution. In: Selim, In.H.H., Ma, L. (Eds.), Physical non-equilibrium in soils: Modeling and application. Ann Arbor Press, pp. 195–221.
[48] Jarvis, N.J., 2007. A review of non-equilibrium water flow and solute transport in soil macropores: principles, controlling factors and consequences for water quality. Eur J Soil Sci 58 (3), 523–546. https://doi.org/10.1111/j.1365-2389.2007.00915.x.
[49] Majdalani, S., Michel, E., Di-Pietro, L., Angulo-Jaramillo, R., 2008. Effects of wetting and drying cycles on in situ soil particle mobilization. Eur J Soil Sci 59 (2), 147–155. https://doi.org/10.1111/j.1365-2389.2007.00964.x.
[50] Majdalani, S., Michel, E., Di Pietro, L., Angulo-Jaramillo, R., Rousseau, M., 2007. Mobilization and preferential transport of soil particles during infiltration: a core-scale modeling approach. Water Resour Res 43 (5), 1–14. https://doi.org/10.1029/2006WR005057.
[51] Shang, J., Flury, M., Chen, G., Zhuang, J., 2008. Impact of flow rate, water content, and capillary forces on in situ colloid mobilization during infiltration in unsaturated sediments. Water Resour Res 44 (6), 1–12. https://doi.org/10.1029/2007WR006516.
[52] Schelde, K., Moldrup, P., Jacobsen, O.H., de Jonge, H., de Jonge, L.W., Komatsu, T., 2002. Diffusion-limited mobilization and transport of natural colloids in macroporous soil. Vadose Zone J 1 (1), 125–136. https://doi.org/10.2136/vzj2002.1250.
[53] Mohanty, S.K., Saiers, J.E., Ryan, J.N., 2015. Colloid mobilization in a fractured soil during dry-wet cycles: role of drying duration and flow path permeability. Environ Sci Technol 49 (15), 9100–9106. https://doi.org/10.1021/acs.est.5b00889.
[54] Peter, L., Modiri-Gharehveran, M., Alvarez-Campos, O., Evanylo, G.K., Lee, L.S., 2025. PFAS fate using lysimeters during degraded soil reclamation using biosolids. J Environ Qual 54, 41–53. https://doi.org/10.1002/jeq2.20576.
[55] Zeng, J., Guo, B., 2023. Reduced accessible air–water interfacial area accelerates PFAS leaching in heterogeneous vadose zones. Geophys Res Lett 50 (8) e2022GL102655.
[56] Carroll, D., 1959. Ion exchange in clays and other minerals. Geol Soc Am Bull 70 (6), 749–779. https://doi.org/10.1130/0016-7606(1959)70[749:IEICAO]2.0.CO;2.
[57] Dollinger, J., Bourdat-Deschamps, M., Pot, V., Serre, V., Bernet, N., Deslarue, G., et al., 2022. Leaching and degradation of S-Metolachlor in undisturbed soil cores amended with organic wastes. Environ Sci Pollut Res 29 (14), 20098–20111. https://doi.org/10.1007/s11356-021-17204-z.
[58] Sequeira, R., Lung, F., 1995. A critical data analysis and interpretation of the pH, ion loadings and electrical conductivity of rainwater from the territory of Hong Kong. Atmos Environ 29 (18), 2439–2447.
[59] Pires, L.F., Bacchi, O.O.S., Reichardt, K., 2004. Damage to soil physical properties caused by soil sampler devices as assessed by gamma ray computed tomography. Aust J Soil Res 42 (7), 857. https://doi.org/10.1071/SR03167.
[60] Pires, L.F., Bacchi, O.O., Reichardt, K., 2007. Assessment of soil structure repair due to wetting and drying cycles through 2D tomographic image analysis. Soil Tillage Res 94 (2), 537–545. https://doi.org/10.1016/j.still.2006.10.008.
[61] Michel, E., Majdalani, S., Di-Pietro, L., 2014. A novel conceptual framework for long-term leaching of autochthonous soil particles during transient flow. Eur J Soil Sci 65 (3), 336–347. https://doi.org/10.1111/ejss.12135.
[62] Rousseau, M., di Pietro, L., Angulo-Jaramillo, R., Tessier, D., Cabibel, B., 2004. Preferential transport of soil colloidal particles: physicochemical effects on particle mobilization. Vadose Zone J 3 (1), 247–261. https://doi.org/10.2136/vzj2004.2470.
[63] van den Bogaert, R., Cornu, S., Michel, E., 2016. To which extent do rain interruption periods affect colloid retention in macroporous soils? Geoderma 275, 40–47. https://doi.org/10.1016/j.geoderma.2016.04.010.
[64] Gee, G.W., Or, D., 2018. 2 4 Part-Size Anal 255–293. https://doi.org/10.2136/sssabookser5.4.c12.
[65] Simonnet-Laprade, C., Budzinski, H., Maciejewski, K., le Menach, K., Santos, R., Alliot, F., et al., 2019. Biomagnification of perfluoroalkyl acids (PFAAs) in the food web of an urban river: assessment of the trophic transfer of targeted and unknown precursors and implications. Environ Sci Process Impacts 21 (11), 1864–1874. https://doi.org/10.1039/c9em00322c.
[66] Macorps, N., Labadie, P., Lestremau, F., Assoumani, A., Budzinski, H., 2023. Per- and polyfluoroalkyl substances (PFAS) in surface sediments: occurrence, patterns, spatial distribution and contribution of unattributed precursors in French aquatic environments. Sci Total Environ 874, 162493. https://doi.org/10.1016/j.scitotenv.2023.162493.
[67] Daliakopoulos, I.N., Tsanis, I.K., Koutroulis, A., Kourgialas, N.N., Varouchakis, A. E., Karatzas, G.P., et al., 2016. The threat of soil salinity: A European scale review. Sci Total Environ 573, 727–739. https://doi.org/10.1016/j.scitotenv.2016.08.177.
[68] Hartmann, A., 1998. Cation exchange processes in structured soils at various hydraulic properties. Soil Tillage Res 47 (1–2), 67–72. https://doi.org/10.1016/S0167-1987(98)00074-9.
[69] Courtier-Murias, D., Michel, E., Rodts, S., Lafolie, F., 2017. Novel experimental–modeling approach for characterizing perfluorinated surfactants in soils. Environ Sci Technol 51 (5), 2602–2610. https://doi.org/10.1021/acs.est.6b05671.
[70] Zachara, J., Brantley, S., Chorover, J., Ewing, R., Kerisit, S., Liu, C., et al., 2016. Internal domains of natural porous media revealed: critical locations for transport, storage, and chemical reaction. Environ Sci Technol 50 (6), 2811–2829. https://doi.org/10.1021/acs.est.5b05015.
[71] Brusseau, M.L., Rao, P.S., 1989. The influence of sorbate-organic matter interactions on sorption nonequilibrium. Chemosphere 18 (9-10), 1691–1706. https://doi.org/10.1016/0045-6535(89)90453-0.
[72] Sprague, L.A., Herman, J.S., Hornberger, G.M., Mills, A.L., 2000. Atrazine adsorption and colloid-facilitated transport through the unsaturated zone. J Environ Qual 29 (5), 1632–1641. https://doi.org/10.2134/jeq2000.00472425002900050034x.
[73] Jacobsen, O., Moldrup, P., Larsen, C., Konnerup, L., Petersen, L., 1997. Particle transport in macropores of undisturbed soil columns. J Hydrol 196 (1-4), 185–203. https://doi.org/10.1016/S0022-1694(96)03291-X.
[74] Auset, M., Keller, A.A., Brissaud, F., Lazarova, V., 2005. Intermittent filtration of bacteria and colloids in porous media. Water Resour Res 41 (9), 1–13. https://doi.org/10.1029/2004WR003611.
[75] Flury, M., Aramrak, S., 2017. Role of air-water interfaces in colloid transport in porous media: a review. Water Resour Res 53 (7), 5247–5275. https://doi.org/10.1002/2017WR02059.
[76] Denovio, N.M., Saiers, J.E., Ryan, J.N., 2004. Colloid movement in unsaturated porous media: recent advances and future directions. Vadose Zone J 3.2, 338–351. https://doi.org/10.2136/vzj2004.0338.
[77] Saiers, J.E., Hornberger, G.M., Gower, D.B., Herman, J.S., 2003. The role of moving air-water interfaces in colloid mobilization within the vadose zone. Geophys Res Lett 30 (21), 2083. https://doi.org/10.1029/2003GL018418.
[78] Gerke, H.H., 2006. Preferential flow descriptions for structured soils. J Plant Nutr Soil Sci 169 (3), 382–400. https://doi.org/10.1002/jpln.200521955.
[79] Govindaraju, R.S., Reddi, L.N., Kasavaraju, S.K., 1995. A physically based model for mobilization of kaolinite particles under hydraulic gradients. J Hydrol 172 (4). https://doi.org/10.1016/0022-1694(95)02737-A.
[80] Israelachvilli, J., 1992. Intermolecular and surface forces. Academic Press Inc, San Diego.
[81] Lindstrom, A.B., Strynar, M.J., Libelo, E.L., 2011. Polyfluorinated compounds: past, present, and future. Environ Sci Technol 45 (19), 7954–7961. https://doi.org/10.1021/es2011622.
[82] Bräunig, J., Baduel, C., Barnes, C.M., Mueller, J.F., 2019. Leaching and bioavailability of selected perfluoroalkyl acids (PFAAs) from soil contaminated by firefighting activities. Sci Total Environ 646, 471–479. https://doi.org/10.1016/j.scitotenv.2018.07.231.
[83] Anderson, R.H., Feild, J.B., Dieffenbach-Carle, H., Elsharnouby, O., Krebs, R.K., 2022. Assessment of PFAS in collocated soil and porewater samples at an AFFF-impacted source zone: Field-scale validation of suction lysimeters. Chemosphere 308, 136247.
[84] Klamerus, J., Khan, K., Hire, M., Lee, L.S., Schaefer, C.E., 2025. Field measurement of PFAS leaching at a long-term land-applied biosolids site. Environ Sci Technol 59 (38), 20675–20683.
[85] Dorrance, D.W., Wilson, L.G., Everett, L.G., Cullen, S.J., 1991. Compendium of in situ pore-liquid samplers for vadose zone (ACS Symposium Series). In: Nash, R.G., Leslie, A.R. (Eds.), Groundwater Residue Sampling Design, 1991. American Chemical Society, Washington, DC.
[86] Sörengård, M., Franke, V., Tröger, R., Ahrens, L., 2020. Losses of poly-and perfluoroalkyl substances to syringe filter materials. J Chromatogr A 1609, 460430.

Glossary

6:2 FTAB: 6:2 Fluorotelomer sulfonamide betaine
6:2 FTSA: 6:2 Fluorotelomer sulfonic acid
8:2 FTSA: 8:2 Fluorotelomer sulfonic acid
10:2 FTSA: 10:2 Fluorotelomer sulfonic acid
AFFF: Aqueous Film Forming Foam
AWI: Air Water Interface
Br-FOSA: Branched Perfluorooctane sulfonamide
Br-PFOS: Branched Perfluorooctanesulfonic acid
CEC: Cation Exchange Capacity
Concentration: amount per mass of liquid
Content: amount per mass of solid
CT: Computed Tomography
FOSA: Perfluorooctane sulfonamide
FOSAA,: Perfluorooctane sulfonamidoacetic acid
FPePA,: 2 H,2 H,3 H,3H-Perfluorooctanoic acid
ICP–OES: Inductively Coupled Plasma–Optical Emission Spectroscopy
ISO: International Organization for Standardization
LC-ESI-MS/MS: Liquid Chromatography Electrospray Ionization tandem Mass Spectrometry
Leaching: Process in which a liquid solvent removes soluble substances from a porous medium
LoD: Limit of Detection
L-PFOS: Linear Perfluorooctanesulfonic acid
n_c: length of the perfluorinated carbon chain
PFAS: Per- and polyfluoroalkyl substances
PFBA: Perfluorobutanoic acid
PFBS: Perfluorobutanesulfonic acid
PFCA: Perfluorocarboxylic acids
PFDA: Perfluorodecanoic acid
PFDoDA: Perfluorododecanoic acid
PFDS: Perfluorodecanesulfonic acid
PFHpA: Pefluoroheptanoic acid

PFHxA: Perfluorohexanoic acid
PFNA: Perfluorononanoic acid
PFOA: Perfluorooctanoic acid
PFOS: Perfluorooctanesulfonic acid
PFPeA: Perfluoropentanoic acid
PFSA: Perfluorosulfonic acids
PFTeDA: Perfluorotetradecanoic acid
PFTrDA: Perfluorotridecanoic acid
PFUnDA: Perfluoroundecanoic acid
Release: release is more general than leaching and applies for both solute and colloids
RID: Rain Interruption Duration
TOC: Total Organic Carbon
USDA: United States Department of Agriculture.
XRD: X-ray diffraction